# Supplementary material to "Spectral optical properties of soot: laboratory investigation of propane flame particles and their link to composition"

5 **Figure S1. Example illustrating the statistical analysis performed on MAC measurements. a) Gaussians probability (Eq. 7) stacking of measured MAC values. Data shown correspond to CS1 observations. S1b) shows the total ensemble of PDFs for all measured CS1 MAC values. The text on top of the figure reports the number of soot generations corresponding to CS1 analysis, in this case 13 (Gen.=13), and the number of single 3-minute MAC observations in the ensemble of experiments (n=600, which are stacked with a resolution of 0.01 m²g⁻¹ and shown in b). S1a) shows then the sum of all Gaussians in b) and fitted Gaussians**
10 **distribution to the sum of all Gaussian values providing the count median supplied in the header of the graphic.**
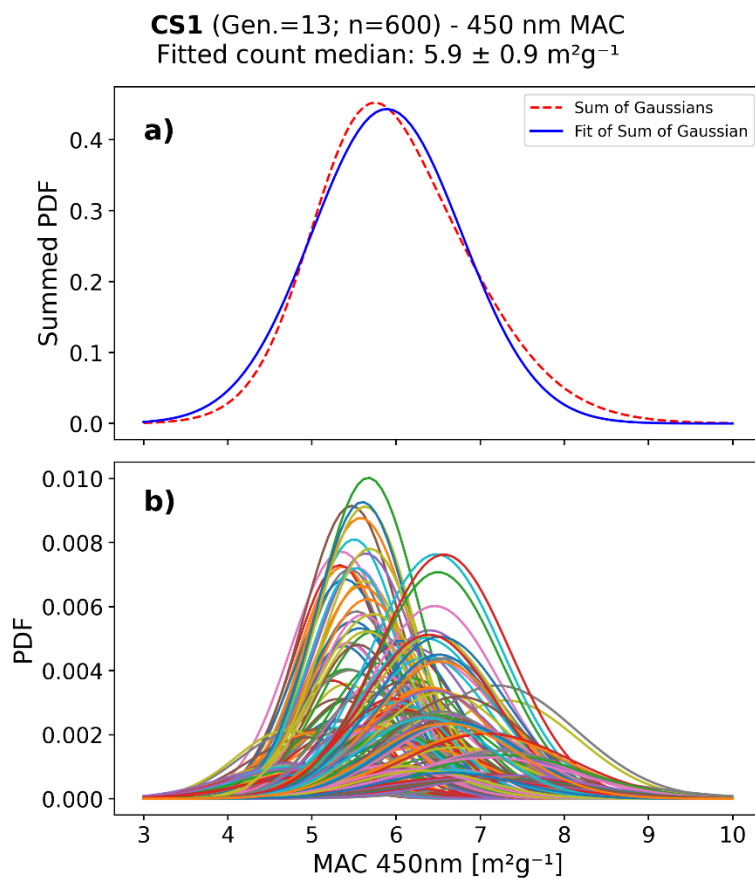
Figure S2. Alternative plot for Fig. 4: Sum of Gaussians of MAC/MSC/MEC values and fitted Gaussians distribution of the sum for CS1 to CS5 at 630 nm. For each plot the soot, together with their number of generations, and used data points (n) is given. Further, the mean value of the peak together with its standard deviation is provided, determined from the fit of Eq. (7).
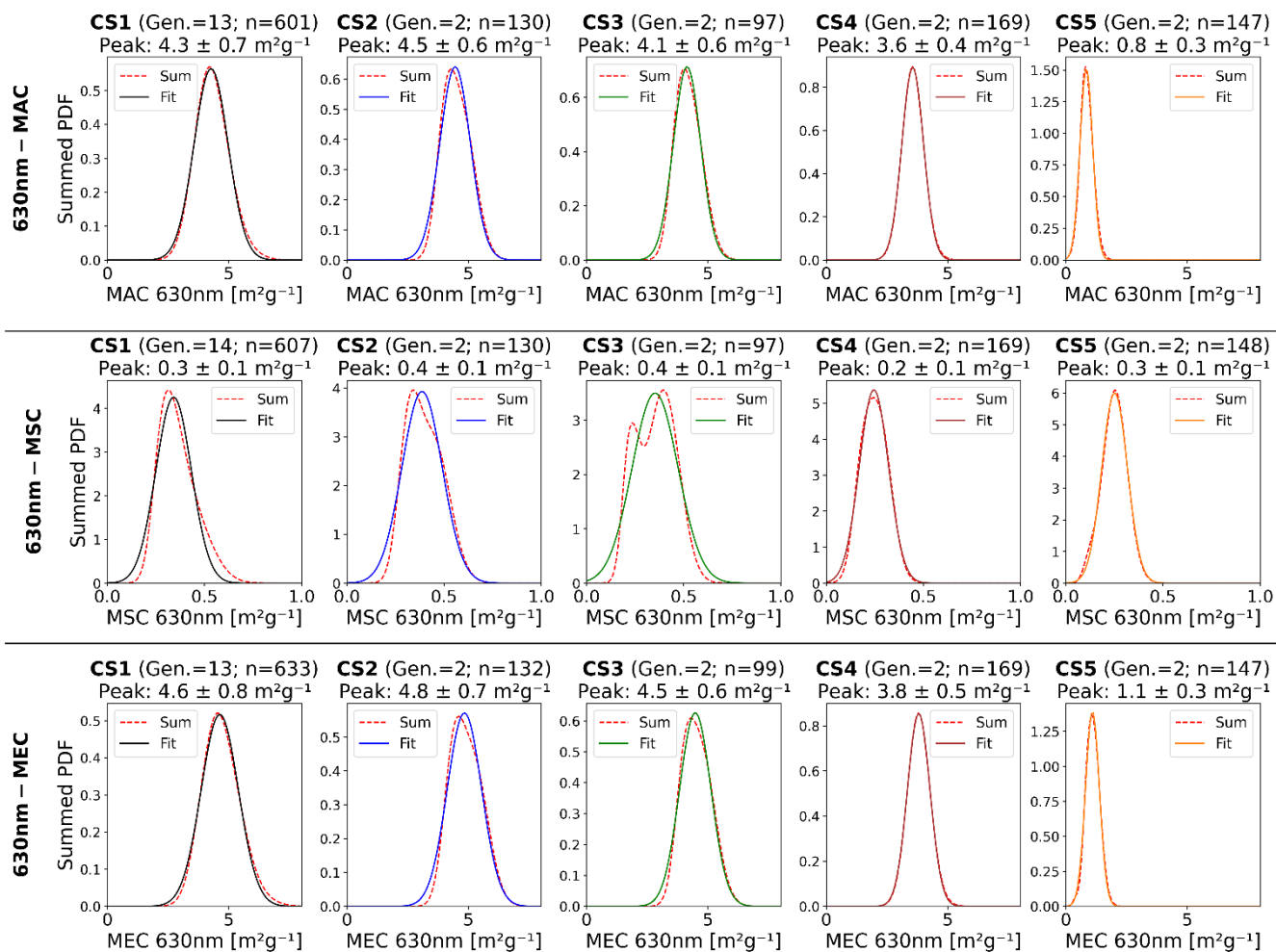
Figure S3. Alternative plot for Fig. 7: Compositional dependent absorption mass absorption and scattering cross sections and their spectral variability represented by the AAE and SAE. The MAC data obtained in the present study at 550 nm (green points) are combined with observations from past literature and put in relation to the EC/OC soot content. Data retrieved as described for Fig.7. The EC/OC ratios, if not available from the original publication, were determined using EC+OC=TC assumption, thus $\frac{OC}{TC} = 1 - \frac{EC}{TC}$, and $\frac{EC}{OC} = \frac{EC}{TC}\frac{TC}{OC}$. In case no uncertainties for EC, OC, or TC were given, the EC/TC uncertainty was assumed to be true for OC/TC and then propagated (resulting in potential underestimations of the EC/OC uncertainty).
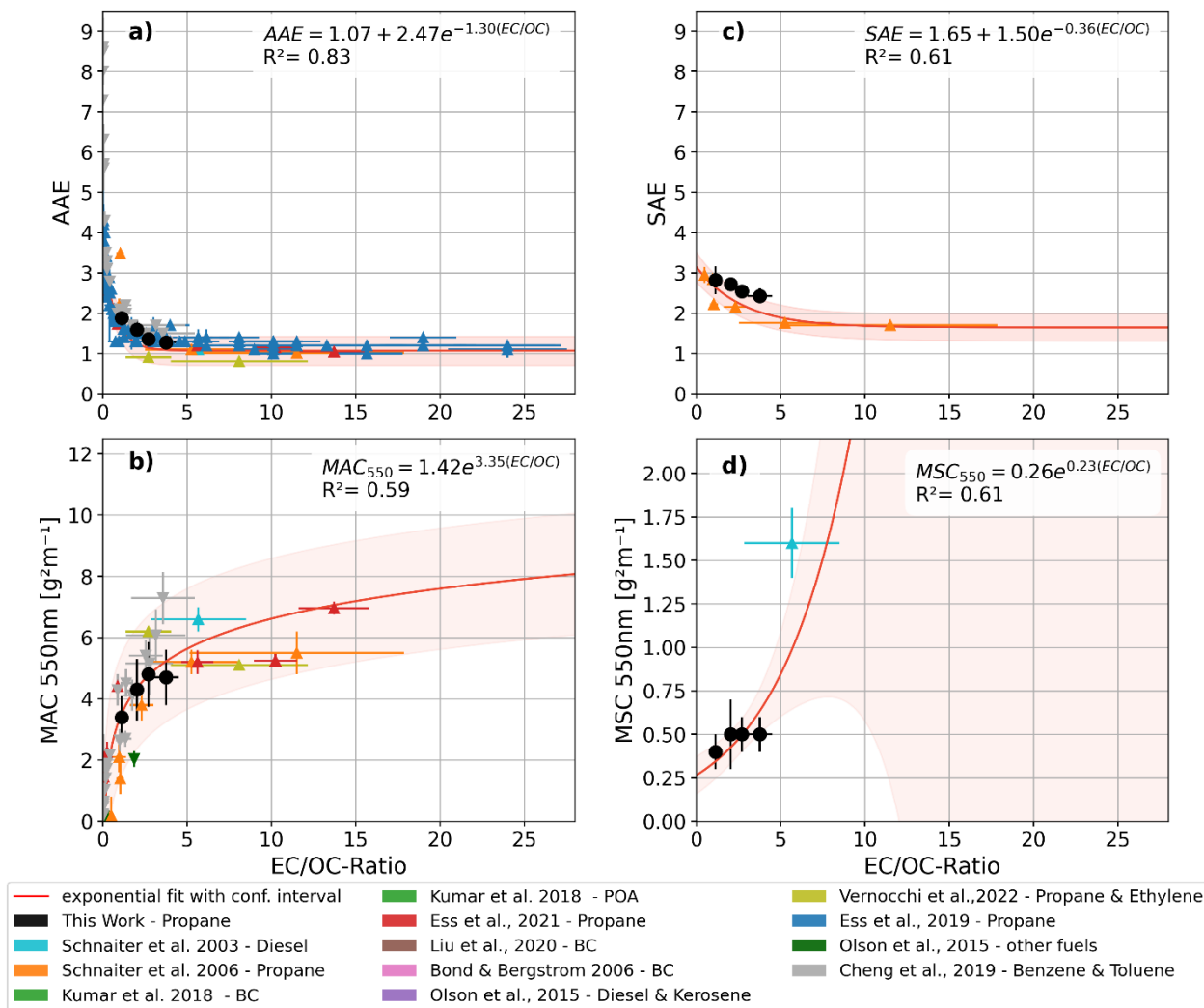
30 **Figure S4. Representative example of the measurements of mass concentration of ammonium sulphate. Comparison of mass concentration in µg m^{-3} from the TEOM (green line) and calculated using the SMPS, assuming spherical particles and using density from the literature (red line; 1.8 g cm^{-3} (e.g. Bond and Bergstrom (2006)) and as measured from the CPMA-system (grey line). The black line marks the beginning of the injection.**
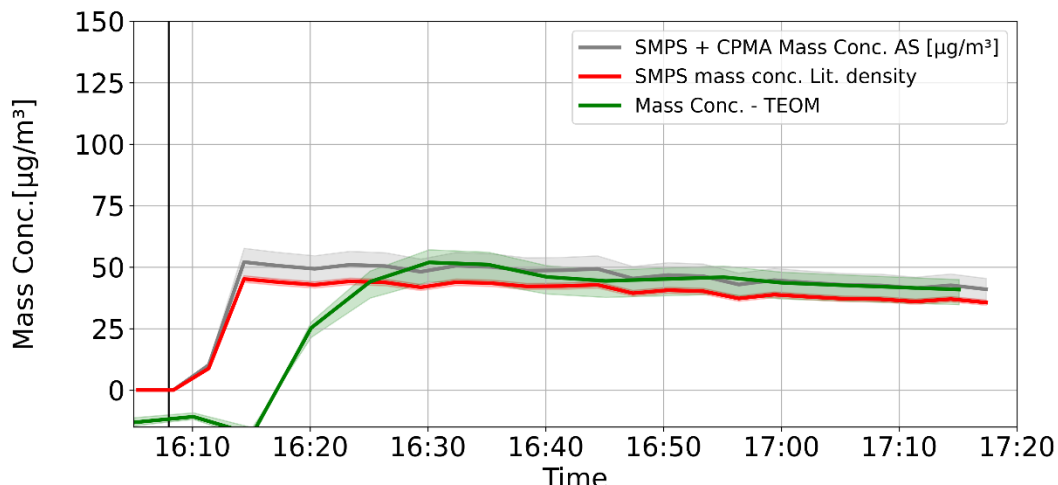
35

Figure S5. Representative example of the measurements of optical properties of ammonium sulphate experiment. Comparison of the extinction and scattering signals determined at 450 and 630 nm with their uncertainties as shaded areas. The black line marks the injection. Note that the optical instruments are not connected simultaneously and thus differ in their start of measurement.

40

4
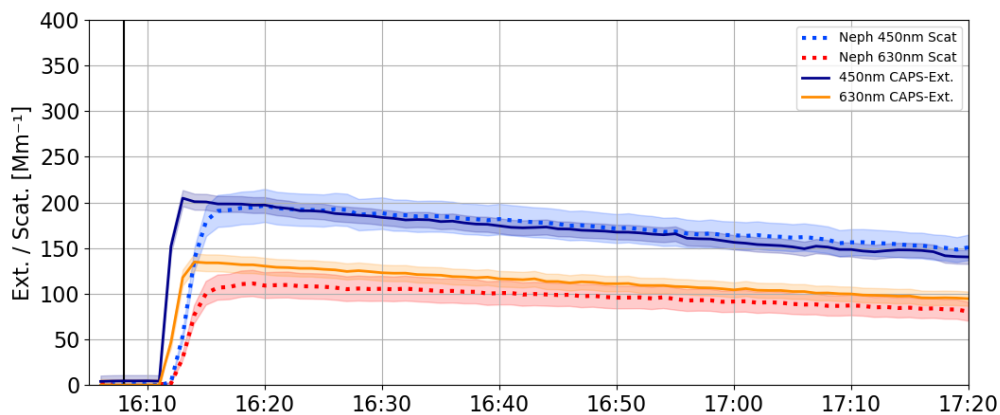
Table S1. Full list of CESAM soot experiments analysed in the present work. Additional information includes the length of the measurement interval for acquisition of the properties of fresh soot (data basis for this paper), total soot lifetime inside the chamber, and initial mass concentration injected into the chamber. Further, the table includes information on additional ageing conditions and injections of different compounds such as water (measured as relative humidity RH), ozone, SO₂, and α-pinene, used to investigate the impact of ageing conditions on soot aerosol properties. These ageing conditions are not considered in the present work.

Experiment	Meas. interval fresh soot (hh:mm)	Total Lifetime (hh:mm)	Initial mass concentration [µg m⁻³]	RH	O3 [ppb]	SO₂ or α-pinene [ppb]	Date
CS lifetime experiments (dry, dark) – Fresh and aged under the effect of coagulation							
CS1 Lifetime 1	21:51	21:51	63 ± 6	/	/	/	23/02/2021
CS1 Lifetime 2	25:36	25:36	198 ± 18	/	/	/	24/02/2021
CS1 Lifetime 3	05:56	05:56	61 ± 6	/	/	/	19/10/2021
CS2 Lifetime 1	03:05	03:05	99 ± 8	/	/	/	11/03/2021
CS2 Lifetime 2	05:05	05:05	95 ± 8	/	/	/	20/10/2021
CS3 Lifetime 1	01:51	01:51	58 ± 5	/	/	/	11/03/2021
CS3 Lifetime 2	04:32	04:32	89 ± 8	/	/	/	26/10/2021
CS4 Lifetime 1	02:59	02:59	23 ± 2	/	/	/	12/03/2021
CS4 Lifetime 2	06:25	06:25	44 ± 4	/	/	/	22/10/2021
CS5 Lifetime 1	03:53	03:53	46 ± 4	/	/	/	28/05/2021
CS5 Lifetime 2	05:52	05:52	65 ± 7	/	/	/	21/10/2021
CS chemically aged experiments (e.g. 30% RH, light, oxidant)							
CS1 + hv 1	02:56	05:01	67 ± 6	/	/	/	17/05/2021
CS1 + hv 2	01:34	02:37	58 ± 6	/	/	/	19/05/2021
CS1 + H2O	01:55	07:11	78 ± 8	≈ 30%	/	/	26/02/2021
CS1 + H2O + hv	01:32	06:46	79 ± 8	≈ 30%	/	/	01/03/2021
CS1 + O3 + hv	01:42	07:48	74 ± 7	≈ 30%	1345	/	02/03/2021
CS1 + SO2 + hv	01:32	06:50	90 ± 8	≈ 30%	/	272	03/03/2021
CS1 + O3 + SO2 + hv 1	01:37	24:48	89 ± 9	≈ 30%	1437	259	04/03/2021
CS1 + O3 + SO2 + hv 2	02:08	25:16	80 ± 8	≈ 30%	1383	258	09/03/2021
CS1 + O3 + AP	02:01	24:43	63 ± 6	≈ 30%	670	60	18/05/2021
CS1 + O3 + AP - high	02:12	27:03	169 ± 18	≈ 30%	503	120	20/05/2021
CS1 + O3 + AP - low	02:29	07:22	13 ± 2	≈ 30%	559	60	26/05/2021

Table S2. List of key instrumentation used to determine properties of the aerosol particulate phase during the soot experiments in CESAM. Instrument model, measured or derived parameters, time resolution, uncertainty, and main reference or specific data treatment for each technique are provided. For all optical instruments, measurements on HEPA-filter and on the empty chamber were used to determine their current instrumental background noise level, then used to determine the noise-signal-ratio and components of the uncertainty.

Instrument	Measured or derived parameter (units)	Time resolution	Associated Uncertainties		Reference
SMPS System TSI SMPS DMA 3080 & CPC 3772	number size distribution [# cm^{-3}] 19.5 to 881.7 nm	180 s	3% + counting error	Error propagation considering 3% DMA uncertainty in particle mobility size selection plus counting error as the standard deviation of an assumed Poisson distribution	(DeCarlo et al., 2004)
TSI DMA 3080 + CPMA (Cambustion) + CPC 3775 high	P_{eff} (eff. density) [g cm^{-3}] from the mass-resolved number size distribution [# cm^{-3}]	30-45min with 180 s at each mass	10%	Error propagation considering DMA uncertainty, mass-to-charge uncertainty, relative standard error of the size distribution median diameter. For mass calculation, the uncertainty in the power law fit under consideration of the eff. density uncertainties is used	Olfert and Collings (2005) With setup as described by Yon et al. (2015)
TEOM 1400a Thermo Scientific	mass concentration [μg m^{-3}]	300 s	15%	Determined on noise operating on chamber using (determined on clean chamber values and as following smoothed variability)	
CPC 3775 TSI	particle number (> 4 nm) [# cm^{-3}]	1 s	10%	associated uncertainties inside the CESAM system	
SP2 Droplet Measurement Technologies (DMT)	Refractory BC (rBC) mass concentration [μg m^{-3}] rBC number size distribution [# cm^{-3}]	60 s	17%	following the observations by Laborde et al. (2012)	Stephens et al., (2003)

Instrument	Measurement	Time res.	Uncertainty	Uncertainty determination	Reference
Integrating Nephelometer 3563 TSI	scattering coef. [Mm^{-1}] at 450, 550 & 700 nm	1 s	8%	Propagation of uncertainties from cross-calibration (against freshly calibrated Nephelometer), truncation correction, and signal-to-noise ratio (averaged for different total loss conditions)	Description in Anderson et al. (1996) Trunc. corrected using Massoli et al. (2009)
CAPS PM$_{ex}$ Aerodyne	extinction coef. [Mm^{-1}] 2 inst. = 2 wavelength (450, 630nm)	1 s	5-6%	Propagation of uncertainties for general measurement precision (3%, Massoli et al., 2010) and signal-to-noise ratio (averaged for different total loss conditions)	Kebabian et al. (2007) & Massoli et al. (2010)
CAPS PM$_{SSA}$ Aerodyne	extinction coef. [Mm^{-1}] 2 inst. = 2 wavelength (450, 630nm) (only extinction signal used)	1 s	5-6%	Propagation of uncertainties for general measurement precision and signal-to-noise ratio (see above)	Onasch et al. (2015)
CAPS PM$_{ex}$ Aerodyne / Integrating Nephelometer 3563 TSI	absorption coef. [Mm^{-1}] 2 inst. = 2 wavelength (450, 630nm) (extinction minus scattering)	1 s	10-30%	Propagation of uncertainties from the measurements of scattering and absorption including the uncertainties from the interpolation of the scattering signal to 630 nm	
MAAP Thermo-Scientific	absorption coef. [Mm^{-1}] at 637 nm wavelength	60 s	12%	Provided in instruments literature	Petzold and Schönlinner (2004) & Petzold et al. (2005)
TOF - ACSM Aerodyne Research	non-refractory aerosol composition [μg m^{-3}]	360 s	up to 40% (Strongly varying for experiments)	Uncertainty determined from averaged standard deviations of clean air measurements and the intensity of the signal	

Aethalometer (AE33 – dual spot) Magee Scientific	absorption coefficient [Mm^{-1}] 370, 470, 520, 590, 660, 880 950 nm	60 s	12%	Propagation of uncertainty in Pattenuation (following Backman et al. (2017) and using clean air measurements), the Cref, and the loading correction	Drinovec et al. (2015)
MWAA (Multi-Wavelength Absorbance Analyser)	Abs. coef. [Mm^{-1}] at 375, 405, 532,635, 850 nm	15-120 min	mean - 19%	Provided by Massabò and team (var. based on filter loading)	Massabò et al. (2013)
PP_UniMI (Polar photometer)	Abs. coef. [Mm^{-1}] at 405, 448, 532, 635, 780 nm	15-120 min	mean - 14%	Provided by Vecchi and team (var. based on filter loading)	Vecchi et al. (2014)
OCEC Carbon Aerosol Analyzer Sunset Laboratory	elemental carbon organic carbon mass concentration [µg cm^{-2}]	5 sec to 240 min	14%/19%/ 18% average for EC/OC/TC	Uncertainties are determined inside the VBasic-Version OCEC835 analysis software for each thermogram and then propagated	EUSAAR protocol Cavalli et al. (2010)
TEM	morphology	30 sec to 120 min		for D_{pp}, D_f, and k_f as output from Bescond et al. (2014) used average is determined using a single determination of all CS1 pictures	

55

Table S3. List of instrumentation used to characterise the gas phase during the soot experiments in CESAM. Instrument model, measured parameters, time resolution, accuracy, and detection limit of data are given.

Instrument	Parameter (units)	Acquisition resolution (averaged to 1 min)	Accuracy (at 1 min time resolution) & detection limit (Acc./DL)
NO$_x$ Monitor – Horiba APNA370	NO, NO$_2$ (NOx) [ppb]	5 s	1 / 0.5 ppb
APEE - ProCeas	CO/CO$_2$ [ppm]	45 s	0.1/ 0.05 ppm
SO$_2$ Monitor - Horiba APSA370	SO$_2$ [ppb]	5 s	1/ 0.05 ppb
Ozone (O$_3$) Monitor - Horiba APOA370	O$_3$ [ppb]	5 s	1 / 0.05 ppb
Teledyne T500U	NO$_2$ [ppb]	30 s	0.5% (above 5 ppb)/ 0.04 ppb
Hygrometer - Vaisala HMP234	RH [%] & T [°C]	1 s	2% & ± 0.1 °C (only Acc.)
Baratron type MKS 626AX13TDE (high)/ 626AX11TDE (low)	Pressure [mBar]	1 s	0.25% for 1 to 1000 Torr (Unc.)
PTR-ToF-MS (Kore ltd.)	Mass-loading gaseous components [ppb]	60 s	0.1 ppb [DL]

60 **Table S4. Fitting parameters and values for EC/TC-fit of Fig.7. Fitting parameters correspond to the equation $a * e^{(b*EC/TC)}$ for MAC and MSC and $a + b * e^{(-c*EC/TC)}$ for AAE and SAE.**

		Fitting parameters		
		A	B	C
MAC	Central values	1.34	1.77	/
	Uncertainty	0.05	0.10	/
AAE	Central values	3.29	2.32	0.73
	Uncertainty	0.12	0.30	0.12
MSC	Central values	0.15	1.83	/
	Uncertainty	0.11	1.00	/
SAE	Central values	-4.70	8.57	0.29
	Uncertainty	49.16	48.64	1.94

Table S5. Fitting parameters and values for OC/TC-fit of Figure S3. Fitting parameters corresponds to the equation $a * e^{(b*OC/TC)}$ for MAC and MSC and $a + b * e^{(-c*OC/TC)}$ for AAE and SAE.

		Fitting parameters		
		A	**B**	**C**
MAC	Central values	1.42	3.35	/
	Uncertainty	0.23	0.39	/
AAE	Central values	1.07	2.47	1.30
	Uncertainty	0.01	0.14	0.13
MSC	Central values	0.26	0.23	/
	Uncertainty	0.07	0.08	/
SAE	Central values	1.65	1.50	0.36
	Uncertainty	0.27	0.37	0.26

Table S6. List of control experiments and key parameters like relative humidity, and the lifetime in the chamber. The mass concentration is calculated using averages of measured densities applied to SMPS measurement

Experiment	Lifetime in dry conditions (hh:mm)	Total Lifetime (hh:mm)	Est. Initial mass concentration* [$\mu g\ m^{-3}$]	RH	Date
$(NH_4)_2SO_4$ - AS 1	00:42	01:36	80.0	$\approx 30\%$	05/03/2021
$(NH_4)_2SO_4$ - AS 2	01:21	01:21	48.6	<2%	10/03/2021
$(NH_4)_2SO_4$ - AS 3	00:43	00:43	185.3	<2%	18/10/2021
H_2SO_4 – SA 1 *(generated as a secondary aerosol)*	*Generate in a humid environment*	03:21	Peak at 54.9	$\approx 30\%$	08/03/2021

Text S1. Injection of soot aerosols in CESAM

The injection of CS aerosol in CESAM was performed by connecting the miniCAST generator output directly to the chamber through an activated carbon denuder. The flame of the miniCAST was let to stabilize for around 2 to 5 minutes prior to injection. A T-connection was placed at the exit of the miniCAST, whose output flow rate is approximately 7 L min^{-1} for all OP points: one of the T exits was connected to CESAM through an activated carbon denuder (optimized for a flow rate of 3 to 6 L min^{-1}), while the second T exit acted as an exhaust system used for the stabilization period and for the remaining flows during the injection process. Two protocols, that generated soot aerosol with the same properties, were used

to inject the soot into the chamber: one where the pressure and compensation of the chamber were adjusted to pull with a constant flow of 5 L min^{-1} while the remaining flow (approximately 2 L min^{-1}) was removed via the exhaust and the second one where the exhaust was closed during injection and the outflow of the miniCAST (7 L min^{-1}) was used to push the aerosol against a slight pressure gradient through the denuder into the chamber. The activated carbon denuder was used to minimize the potential injection of volatile organic compounds from the flame exhaust into the chamber and therefore limit any chemical processing of the CS aerosol after the initial combustion process. All connections between the miniCAST and the chamber are made of half-inch stainless steel tubing. To note that during soot injection some of the aerosol online instrumentation was disconnected to avoid any possible damages due to eventual short pressure changes.

Text S2. Control experiments

Four control experiments were performed using ammonium sulphate (AS - $(NH_4)_2SO_4$) and sulfuric acid (SA - H_2SO_4) to validate and characterize the instrumentational setup, in particular, the optical instrumentation and the mass concentration dataset. Both compounds are largely available atmospheric components and therefore the physico-chemical properties including spectral optical properties have been intensively studied (e.g. Toon et al., 1976; Flores et al., 2009), in particular also inside the CESAM chamber system (e.g. Denjean et al., 2014). The aerosols are considered to be more or less spherical and non-absorbing which are key properties for the validation of the optical properties as they fit well with the approximation of spherical homogeneous particles for Mie calculations. The non-absorption properties were used to verify that the measured values from the EMS devices agree, meaning $b_{scat}=b_{ext}$ and consequently b_{abs} equals zero.

The ammonium sulphate aerosol was generated from a 0.03M solution (ultrapure water, ≤3.0 ppb of TOC, and Ammonium sulfate, 99.9999% Suprapur®, Merck) using a constant-output atomizer (Model 3076, TSI) operated at a flow rate of 2 L min^{-1}. The sulfuric acid aerosol was generated by injecting SO_2 (about 270 ppb) in an O_3-rich (1 ppm) humid (>30%) environment and afterwards starting the photo-chemical generation of OH by adding the radiation using three 6.5 kW-xenon-arc lamps through three quartz windows with 6.5 mm-thick Pyrex® filters.

The number size distribution measurements from the SMPS allowed indirect determination of the theoretical extinction and scattering coefficients using Mie theory calculations and refractive indexes assumed from the literature. For spherical particles, as we consider for AS and SA, the mobility diameter of the SMPS can be assimilated to a volume-equivalent diameter (i.e., shape factor equal to 1). On the other hand, Mie calculations can be also used to provide an inverse determination of the refractive index of the aerosol: starting from the measured number distribution and scattering and extinction coefficients, the refractive index of the aerosol can be determined as the value that allows to most closely reproduce the measured optical signals. Mie calculations were done at 3 wavelengths (450, 550, 630 nm) using the b_{scat}, b_{ext}, and b_{abs} from the EMS methods and using extrapolation based on $b_{ext,550} = b_{ext,\lambda_1} * (\frac{\lambda_1}{550})^{AEE_{approx}}$ with $AEE_{approx} = -\frac{\log(\frac{MAC_{\lambda_1}}{MAC_{\lambda_2}})}{\log(\frac{\lambda_1}{\lambda_2})}$ to approximate the extinction at 550 nm and the scattering at 630 nm from the measurements. The SPMS number

size distribution together with scans of the DMA-CPMA-CPC system and data from the TEOM, as described in the main manuscript, were additionally used to test and verify the effective density measurements to compare them against available values in literature and check the consistency of mass concentration measurements.

Effective density measurements. The measurements of the effective densities of AS and SA on average were 1.89 ± 0.19 g cm-3 and 1.64 ± 0.16 g cm-3 (size-independent). These values were found to deviate, but still to agree within uncertainties, from the expected values of 1.76 and 1.8 g cm-3 (Hand and Kreidenweis, 2002; Myhre et al., 1998; Tang, 1996) proposed in the literature for the pure and dry compounds. To note however that CESAM values were measured in a humid environment, a condition possibly affecting the aerosol density. For the sulphuric acid in particular the influence of the >30% relative humidity in the chamber reduces the effective density of the aerosol due to the dilution of the acid by the water content in the chamber (Peng et al., 2022), with expected reduction of the density to values around than 1.68-1.7 g cm-3 (Myhre et al., 1998). These results suggest precision and repeatability of the effective density measurements within the provided uncertainty of around 10%.

Mass concentration. Ammonium sulphate experiments were used to validate mass concentration measurement by comparing the masses calculated with the SMPS using both the CPMA-measured effective density and the literature density against the mass measured with the TEOM (see Fig. S4). The comparison indicates a very good agreement in mass concentration measurements between the two techniques, with a better agreement when CPMA-derived effective density, instead of the literature values, is used to calculate the mass concentration from number distribution data.

Optical properties. Figure S5 shows the scattering and extinction coefficients for the ammonium sulphate experiment coded as $(NH4)_2SO4$ - AS 2 (dry conditions). The comparison shows that the nephelometer scattering and the CAPS extinction signals, both at 450 and 630 nm agree within their measurement uncertainty, supporting the consistency of measurements. Despite these observations, a slight systematic difference in the signals of extinction and scattering can be noticed that results in a small absorption signal (of the order of 10 Mm^{-1} from the data shown in Fig. S5) for the EMS-techniques. This is however captured inside the given uncertainties of the absorption coefficient. The results are similar for the other experiments including the sulphuric acid and, despite showing a slight experiment-to-experiment variability, the scattering and extinction agree on average within 9% to 19%, for 450 and 630 nm, respectively, with the highest difference observed at 630 nm. For the sulphuric acid control experiments, low signal strength for scattering and extinction, below 4 Mm^{-1} at 630nm, increases the uncertainties and relative differences for the measurements which are thus not considered in this comparison as they are significantly lower than observed conditions.

Optical calculations with Mie theory were performed to retrieve the refractive indexes for AS and SA aerosols. For the ammonium sulphate, a wavelength-independent average complex refractive index of 1.49 (± 0.09) + i0.008 (± 0.011) was determined at the three wavelengths. While the values of the real part for AS lay inside the expected values of literature, which vary around 1.5 (Denjean et al., 2014; Toon et al., 1976), the imaginary part shows a slightly nonzero value which we attribute to the identified small absorption signal from EMS calculation. For the sulphuric acid a CRI of 1.24 (± 0.05) + i0.004 (± 0.007) was determined with this showing slightly lower values of the real part than expected from the literature

(around 1.36 to 1.4, (Palmer and Williams, 1975), potentially associated to the humidity effect discussed above, and a small non-zero imaginary part.

Summarizing, the control experiments showed that agreement between the different mass measurements is given and that measured effective densities agree within the range of their uncertainties with the literature values. For the optical properties it was shown that the instruments measuring the scattering and extinction despite very well agreeing within their uncertainty, they do not show perfectly equal values, which determine a small but quantifiable absorbing signal for a purely scattering aerosol. While this absorption signal is within measurement uncertainties and therefore not expected to influence the MAC estimates significantly, it can result in a slight bias for the determination of the CRI using optical calculation. Nonetheless, as we expect the CRI of soot to be two orders of magnitude higher than the 0.004-0.008 obtained in control experiments, the impact of this bias is very reduced.

Text S3. Extraction procedure and HPLC-UVVis-ESI/HRMS measurements

The CS particles collected on quartz-fiber filters were extracted to perform HPLC-UVVis-ESI/HRMS analysis. For the extraction procedure, 3 punches of 16 mm each were taken from the 47 mm filter and sonicated in 3 ml of acetonitrile (Fujifilm Wako pure chemical, code: 012-19851, Lot no. ACN 3706). Sonication was performed at 500 rpm for 1h (IKA VIBRAX VXR basic). In order to minimize the exposure to ambient light and so photo-induced reactions during sonication the glass tubes containing the filter samples were covered with aluminium foil. The liquid extracts were then filtered via a PTFE 13 mm-diameter 0.22 mm pore syringe filter (Membrane Solutions) to remove insoluble components and transferred into a glass tube. The resulting solutions were first evaporated (centrifugation at a pressure of 10 kPa at 25°C for about 3 hours; EYELA CVE 2200). Next, 100 µL of acetonitrile was added to get a concentrated solution for HPLC analysis. The obtained solution was homogenized by passing it in an ultrasonic bath for a few seconds. Amber HPLC vials were used to store the solution, which was kept in a freezer at -20°C until analyses. Visual inspection of the filters after acetonitrile extraction indicated remaining material on the filter. This material, mostly of black colour, was assimilable to the remaining insoluble BC on the filters. However, in order to evaluate the presence of any remaining soluble material, sequential extraction in methanol (Fujifilm Wako pure chemical, code: 134-14523, Lot no. TPL 5393) was performed on dried filters for CS1, CS3, and CS5 soot following the same procedure as for acetonitrile extraction. Between extraction and HPLC measurements, the solutions were stored in a freezer.

The analysis of samples was conducted using a High Performance Liquid Chromatography (HPLC; Agilent 1260 infinity) system coupled with a photodiode array (PDA, 190−640 nm, 2 nm resolution) spectrophotometer and a high-resolution mass spectrometer (JEOL JMS-T100LP AccuTOF LC-plus, electrospray ionization high-resolution time-of-flight mass spectrometer; ESI−HRTOFMS) to examine the chemical composition of aerosols. The HPLC separation was carried out on a Proshell 120, EC-C18 column, 3.0×50 mm, with 2.7 μm particle sizes and 120 Å pores, with the temperature set to 30 °C at

a flow rate of 0.2 mL/min. The mobile phase consisted of water (eluent A; purification by MilliQ) containing 0.1% formic acid and acetonitrile (eluent B; Fujifilm Wako pure chemical, code: 012-19851, Lot no. ACN 3706). The gradient elution was programmed as follows: 0−5 min 99% eluent A and 1% eluent B; 5−16 min linear ramp to 100% eluent B; 16−24 min hold at 100% eluent B; 24−25 min return to 99% eluent A and 1% eluent B; 25−39 min hold at 99% eluent A and 1% eluent B. The analysis ends at 30 min. The mass spectrometer was operated with a spray voltage of -2 kV and a resolving power of $m/\Delta m = 6000$. Analysis was done both in negative and positive ion mode. The HPLC−UV/Vis−ESI/HRMS measurement sequence was the following: first only mobile phase without injection is measured, then only acetonitrile pure solution, followed by blanc sample and the CS1 to CS5 samples sequentially.

The obtained UV-Vis absorbance spectra ($Abs(\lambda)$) are treated as follows. First, the raw spectra of both pure solvent (acetonitrile, methanol) and sample are referenced to measurements between 620 and 640 nm, a region assumed to be free of absorption:

$$Abs_{sample}(\lambda) = Abs_{sample-raw}(\lambda) - Abs_{sample-raw}(620-640\ nm) \tag{S1}$$

$$Abs_{solvent}(\lambda) = Abs_{solvent-raw}(\lambda) - Abs_{solvent-raw}(620-640\ nm) \tag{S2}$$

This baseline correction is done to correct for any possible instrumental drift potentially affecting the signal. The solvent absorbance is then subtracted from the sample signal to isolate the signatures of the elute, as:

$$Abs_{sample-elute}(\lambda) = Abs_{sample}(\lambda) - Abs_{solvent}(\lambda) \tag{S3}$$

For CS1, CS3, and CS5 for which both acetonitrile and methanol extractions are performed, the total absorbance is calculated as the sum of the two. Nonetheless, absorbance from methanol counts for less than 20% of total absorption and results are shown for the acetonitrile extracts only.